Discrete element simulations and experiments of soil-winged subsoiler interaction

Xuezhen Wang[1], Peng Li[1], Jinpu He[1,2], Wuquan Wei[1,2], Yuxiang Huang[1,2*]

(1. *College of Mechanical and Electronic Engineering, Northwest A&F University, Yangling 712100, Shaanxi, China*;
2. *Shaanxi Engineering Research center for Agricultural Equipment, Yangling 712100, Shaanxi, China*)

Abstract: Understanding soil disturbance behaviors under the impact of the winged subsoiler is critical for designing or optimizing the winged subsoiler (a primary subsoiling tool). In this study, a soil-winged subsoiler interaction model was developed and the effects of winged subsoiler on soil disturbance behaviors were investigated using the discrete element method (DEM) simulations and lab soil-bin tests. The results showed that wings mainly affected the disturbance range and fragmentation degree of soil above them. The draught forces of share section (SS), arc section in the hardpan (ASHP), arc section in the top layer (ASTL) and line section (LS) were accounted for 69.53%, 25.22%, 4.73% and 0.52% of the total draught force of winged subsoiler; the lateral disturbance range from high to low of the soil at different depths followed the ranking: top layer (TL), hardpan disturbed by arc section (HDAS) and hardpan disturbed by share section (HDSS). Wings had the greatest influence on the draught force of ASHP. Adding wings to an arc-shaped subsoiler increased the disturbance areas of HDAS, TL and HDSS by 47.52%, 7.74% and 4.59%, respectively, but meanwhile increased the total draught force by 36%. Compared with a non-winged subsoiler, winged subsoiler had higher soil looseness (15.83%), soil disturbance coefficient (58.59%), furrow width (448.65 mm) and soil disturbance area ratio (0.3835), but poorer soil surface flatness (19.79 mm) and lower soil loosening efficiency (39.35 mm²/N). This study provided critical information for optimizing winged subsoilers on aspects of improving soil loosening effectiveness and reducing draught force.
Keywords: hardpan, winged subsoiler, draught force, soil disturbance, discrete element method (DEM), experiment
DOI: 10.25165/j.ijabe.20211401.5447

1 Introduction

Soil compaction and hardpan limit root penetration, which in turn makes plants more susceptible to drought stress, and reduces the yield[1-3]. Subsoiling helps to disrupt hardpans and overcome soil compaction. For conventional subsoilers (e.g., column or full-range subsoiler), a much larger area of top layer soil is disturbed than that of the hardpan, which is considered as poor performance of tillage operation, as it is most likely to result in excessive moisture evaporation[4,5]. In contrast, a good designed winged subsoiler can disrupt hardpans by the large area without significantly increasing the disturbance area of the top layer soil. This is desired because it favors soil moisture preservation[4,6]. Understanding of soil-winged subsoiler interaction is critical for improving the design of winged subsoilers for conservation tillage.

In the past few decades, investigation on the soil-subsoiler interaction has been carried out mainly through three approaches, i.e., experimental method, analytical method, and numerical method. The experimental method is costly and field tests may only be undertaken certain times a year[7-9]. Analytical methods

are limited by soil failure assumptions and simple tool geometry[3,10]. Numerical method is capable of examining complex tool geometry and soil dynamic attribute[4,7]. With the rapid development of computer technology, the discrete element method (DEM) has been used to simulate soil-subsoiler interaction[4,5,11]. Ding et al.[11] investigated the effect of working depth on deep tillage tool performance under near quasi-static conditions using DEM modelling at the working speed of 0.1 m/s. Huang et al.[5] proposed a subsoiler model using the DEM, which was able to predict the microscopic movement of soil at different positions with a relative error of less than 20%. Tanaka et al.[12] simulated the soil loosening process caused by a vibrating subsoiler based on the DEM. Many of these existing studies used the Hertz-Mindlin with bonding (HMB) model to simulate the cohesive behavior of agricultural soil; however, these studies mainly focused on the interaction between soil and non-winged subsoiler which was a simple soil-engaging tool. In contrast, both the geometry of the winged subsoiler and the microscopic soil loosening process is relatively complicated. However, contact forces (e.g., tool draught and vertical forces) and soil behaviors (e.g., soil displacement and velocity) under the impact of winged subsoiler which is a prerequisite for designing high-performance winged subsoilers, are absent in previous DEM studies.

In this study, the DEM that was implemented in a type of commercial software, experts in Discrete Element Modeling (EDEM, DEM-Solutions Inc., UK), was used to simulate the interaction between a winged subsoiler and soil. The objectives of this study were to (1) develop a DEM model to simulate soil–winged subsoiler interaction using EDEM 2.7; (2) investigate the impact of winged subsoiler on soil dynamic characteristics,

including microscopic soil disturbance process and soil displacements and velocities; (3) compare the performance of winged and non-winged subsoilers on soil looseness, soil disturbance coefficient, soil loosening efficiency and draught force; (4) validate the simulation results using experimental data of soil disturbance and cutting forces.

2   Methods

2.1   Experiment

2.1.1   Description of the equipment and testing facility

The winged subsoiler tested had a pair of adjustable wings as shown in Figure 1.   The cutting share was a chisel tine, and the shank was an arc-shaped edge-on shank selected based on the Chinese standards JB/T 9788-1999[4].

a. Side view

b. Top view
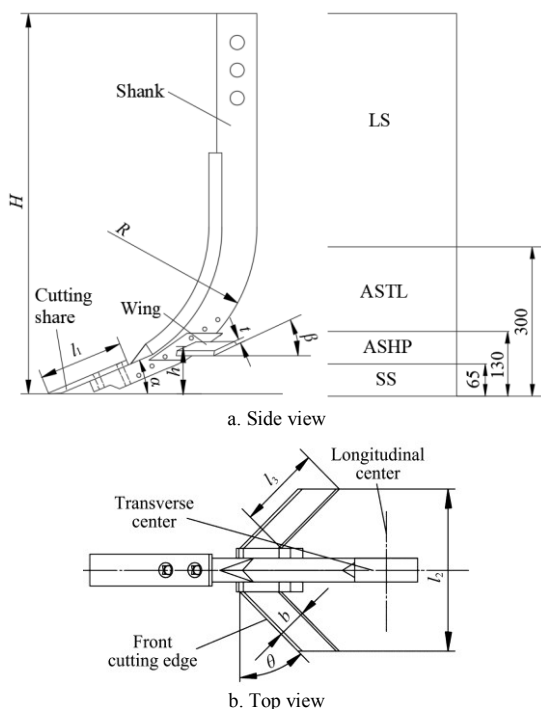
Note: H=770 mm, subsoiler height; h=95 mm, mounting height of wings which is the vertical distance between the bottom of cutting share and the mounting position; R=320 mm, the radius of the curvature of the shank; β=25°, mounting angle which is the angle between the low surface of the wing and the horizontal surface; θ=45°, backward angle which is the angle between the front cutting edge of the wing and the surface perpendicular to shank's lateral surface; t=8 mm, wing thickness; b=35 mm, wing width; α=23°, rake angle; l_1=165 mm, share length; l_2=202 mm, subsoiler width; l_3=105 mm, wing length.   SS represents the share section; ASHP represents the arc section in the hardpan; ASTL represents the arc section in the top layer; LS represents the line section.

Figure 1   Structure and geometrical parameters of the winged subsoiler

The winged subsoiler was tested in an indoor soil bin located in the College of Mechanical and Electronic Engineering, Northwest A&F University, China.   The dimension of the soil bin was 26 m×2.1 m×0.7 m.   The soil in the soil bin was the Lou soil (i.e., sandy loam soil) with 15.67%±0.75% gravel, 74.61%±1.75% sand, 9.13%±1.63% silt and 0.58%±0.09% clay.   It had a granular structure with secondary loess as the parent material and clay as the loamy material.   Lou soil is a typical field soil type in northwest China and is one of the soils that most easily formulate compaction and hardpan which makes plants more susceptible to drought stress[4-6,18,31,34].   The density and cone indexes of shallow layer soil are much lower compared with the deep soil in the field.   The soil is divided into the top layer and hardpan based on the density and soil cone index.   A layered method was used to prepare the

soil in the soil bin to mimic the typical field soil with a top layer and a hardpan (Figure 2a), including spraying water, rotary tilling and compacting[4,13].   After the preparation of soil, the soil cone index was measured by a TE-3 digital-display soil cone index tool (Zhejiang Top Instrument Co., Ltd, China) (Figure 2b).   The thicknesses of the top layer and hardpan were approximately 170 mm and 130 mm, respectively.   The density, water content, and cone index of the top layer were (1404±43) kg/m³, 17.02%±2.34%, and (3564.4±99.9) kPa, respectively.   The corresponding values for the soil in the hardpan were (1833±50) kg/m³, 22.1%±2.66%, and (5695.2±288.9) kPa.   For the subsoil, they were (1763±47) kg/m³, 13.8%±1.08%, and (3965.5±211.3) kPa, respectively.

a. Soil preparation in the soil bin   b. Soil cone index measurement

c. Experimental process
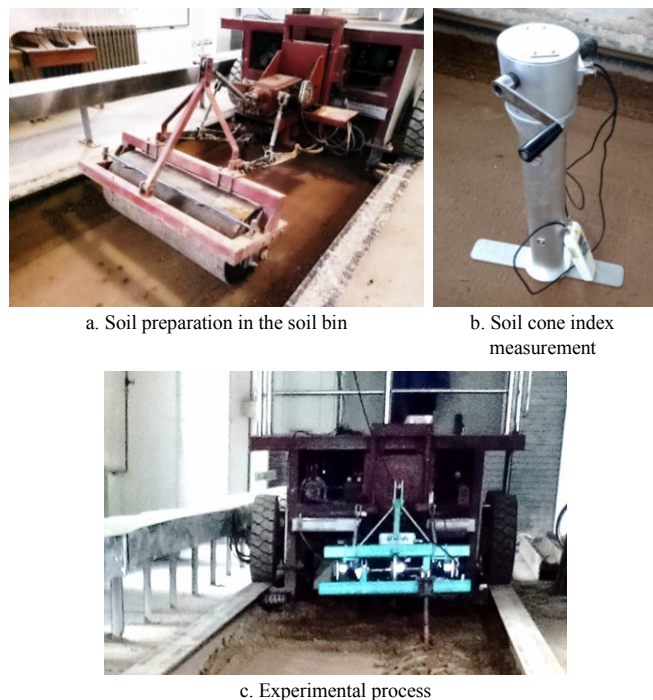
Figure 2   Equipment for tests

2.1.2   Experimental process

The subsoiler and its supporting frame were connected to a TCC electric soil-bin test trolley with a four-wheel drive (Autobona Inc., China)[14] through a three-point hitch (Figure 2c).   The working speed of the trolley was set to approximately 0.83 m/s based on the local subsoiling speed.   The draught force of the winged subsoiler was measured through force sensors and wireless devices placed on the hitch (accuracy: ±0.01 N).   To ensure the stability of the test data, the travel distance with a constant travel speed was used for measurements.

2.2   Measurements

2.2.1   Soil disturbance profile

To measure the soil disturbance profile, after a subsoiling test run, three random locations were chosen in the stable travel section of the soil bin.   A 1500 mm wide profile meter consisting of 150 free-dropping wooden pins was used to measure the soil surface and furrow profiles (Figure 3).   Loose soil in a furrow was firstly excavated manually; then the profile meter was placed in the furrow and the wooden pins were adjusted for their vertical positions automatically according to the contour of the furrow; finally, furrow profiles were traced on engineering graphic paper with the grid spacing of 1 mm, and the furrow area was calculated by the number of grids in the furrow profile multiplying the area of one grid (1 mm²).   The average value of the soil disturbance area of the three selected locations was reported.

Figure 3   Soil disturbance measurement using a profile meter in an excavated furrow

2.2.2   Soil looseness and soil disturbance coefficient

The soil looseness and soil disturbance coefficient can reflect

the soil disturbance of subsoiling[4]. The two parameters were calculated as follows:

$$P = \frac{A_f - A_o}{A_o} \times 100\% \qquad (1)$$

$$\lambda = \frac{A_s}{A_o} \times 100\% \qquad (2)$$

where, P is soil looseness (%), according to Chinese standards JB/T 10295-2001; A_f is the area between soil surface after tillage and theoretical subsoiling bottom before subsoiling, mm^2 (Figure 4a); A_o is the area between the original soil surface and theoretical subsoiling bottom before subsoiling, mm^2 (Figure 4b); λ is soil disturbance coefficient, %; A_s is soil disturbance area between the original soil surface and internal soil disturbance profile, mm^2 (Figure 4c).

a. Area between soil surface after tillage and theoretical subsoiling bottom before subsoiling (A_f)

b. Area between original soil surface and theoretical subsoiling bottom before subsoiling (A_o)

c. Soil disturbance area between original soil surface and internal soil disturbance profile (A_s)

d. Furrow width (l_0), vertical distance from soil surface after tillage to horizontal reference line (a_{kj}); the spacing between two adjacent points (d_0)

Figure 4   Soil disturbance parameters

2.2.3   Soil surface flatness and furrow width

Soil surface flatness and furrow width can be used to evaluate soil disturbance characteristics vertically and laterally, respectively[15-17]. The furrow width l_0 is the width of the maximum soil disturbance (Figure 4d). Soil surface flatness was calculated below[17]:

$$\begin{cases} a_k = \dfrac{\sum_{j=1}^{n_k} a_{kj}}{n_k} \\ S_k = \sqrt{\dfrac{\sum_{j=1}^{n_k} (a_{kj} - a_k)^2}{n_k - 1}} \end{cases} \qquad (3)$$

where, a_k is the average vertical distance from the measured points on the soil surface after tillage to the horizontal reference line in the k-th measurement (k=1, 2, 3, 4, 5), mm; a_{kj} is the vertical distance from the j-th measured point of the soil surface after tillage to horizontal reference line in the k-th measurement, mm; n_k is the number of measured points in the k-th measurement, and the value depends on the width of soil ridge formed after tillage and the spacing between two adjacent points d_0, at here d_0 is 20

mm; $j \leq n_k$; S_k is the soil surface flatness in the k-th measurement, mm (Figure 4d). Soil surface flatness and furrow width after subsoiling were measured at five locations and the average values were reported.

2.2.4   Soil loosening efficiency

Both the minimum of draught force and the maximum of soil disturbance area are desired in subsoiling operations[3]. The soil loosening efficiency is an overall performance indicator considering both the soil cutting force of the subsoiler and its relevant soil loosening characteristics. It was calculated as follows[3]:

$$\eta = \frac{A_s}{F_d} \qquad (4)$$

where, η is the soil loosening efficiency, mm^2/N; F_d is the draught force of the subsoiler, N.

2.2.5   Soil disturbance area ratio

Previous research has shown that reducing the disturbance area of the top layer and increasing the disturbance area of the hardpan is able to regulate the water-holding capacity of the soil[4,6].

Based on the existing data[6], the soil disturbance area ratio was calculated below:

$$\kappa = \frac{A_h}{A_t} \qquad (5)$$

where, κ is the soil disturbance area ratio; A_h is the soil disturbance area of the hardpan, mm²; A_t is the soil disturbance area of the top layer, mm².

3 Discrete element modeling

3.1 Subsoiling model

An appropriate interaction model of soil particles is essential for the accuracy of the DEM simulations. Several studies[4,18] have shown that the bonding (e.g., liquid bridge and cohesive forces) between soil particles significantly affects the tillage resistance and soil disturbance characteristics. Based on the soil type used for the tests, the Hertz-Mindlin with bonding (HMB) model in EDEM 2.7 was selected as the interaction model of particles[4,18].   In this model, bonding contacts were added between particles (Figure 5a) to simulate the cohesive behavior of agricultural soil.   The bond can withstand force and moment; their magnitudes depend on the micro-properties (e.g., critical stress) of the bond.   The bond radius was determined based on the soil moisture content and particle radius[11,13].

a. Cylindrical bonds between particles

b. Discrete element model developed by EDEM
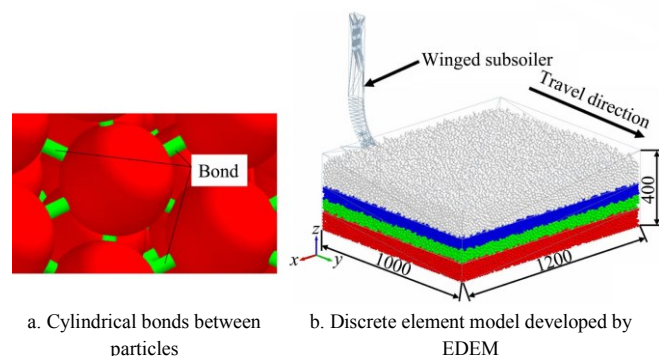
Figure 5   Cylindrical bonds between particles and the discrete element model developed using EDEM

Numerous researchers constructed irregular 3D particle models similar to real granular size and shape by sphere filling and other methods[5,19,20].   However, previous studies have shown that the soil particle shapes are less important when bonds between soil particles are used[7].   Soil particles in the HMB model are bonded together and moved as ''aggregates'', thus the sizes of soil particles will not be critical as long as soil particles are not larger than typical soil aggregates.   Considering aggregate size ranging from 1 to 49 mm for both fine soil and coarse soil[21], many researchers used spheres with a radius of 8 mm or larger as the soil particle model, which still provided accurate predictions[11,13,17,22].   Therefore, the soil particles in this study were chosen to be spherical and had a diameter of 8 mm.

The dimension of the soil bin was set as 1.0 m×1.2 m×0.4 m (length×width×depth).   In the soil domain, the depth of 0-170 mm, 170-300 mm, and 300-400 mm below the soil surface were the top layer, the hardpan, and the subsoil layer, respectively. DEM parameters consist of material and interaction properties. The material properties were obtained from a combination of measurements and available data from literature with the same material of subsoiler (i.e., 65Mn) or similar soil conditions (e.g., soil type and moisture content).   This method has been used in many previous DEM studies[4,11,22,23,25].   The soil density was obtained by measurement.   The shear modulus and Poisson's ratio

of soil and the density and shear modulus of the subsoiler made with 65 Mn steel were from published data[5,13], as shown in Table 1.   The interaction properties mainly consisted of the coefficient of restitution, the coefficient of rolling friction and the coefficient of static friction.   The coefficient of rolling friction between soil and the subsoiler was measured based on the inclined plane test[8,13].   The coefficient of rolling friction in the soil was determined using the angle of repose tests[4,13].   The coefficient of restitution between materials, the coefficient of static friction between soils and the coefficient of static friction between the soil and the subsoiler were obtained from published data[4,13].   The CATIA design software was used to develop a 3D model of the subsoiler used in the tests with a scale of 1:1[18]; then, the 3D model of the subsoiler was imported into the EDEM software (Figure 5b). Finally, the subsoiler was run in the soil domain at a working depth of 300 mm and a working speed of 0.83 m/s.

Table 1   Basic parameters of discrete element model

Parameter	Unit	Value	Source
Density of subsoiler (65Mn steel)	kg/m³	7830	[5]
Poisson's ratio of 65Mn steel	\	0.35	[5]
Shear modulus of 65Mn steel	Pa	7.27×10¹⁰	[5]
Density of top layer soil	kg/m³	1200	Measurement
Poisson's ratio of top layer soil	\	0.40	[13]
Bond stiffness of top layer	N/m³	5×10⁷	[13]
Critical stresses of the bond of top layer	Pa	3×10⁴	[13]
Shear modulus of top layer soil	Pa	6×10⁷	[13]
Radius of the bond of top layer soil	mm	8.54	[13]
Coefficient of rolling friction in top layer soil	\	0.58	Measured by angle of repose test
Coefficient of rolling friction between top layer soil and 65Mn steel	\	0.34	Measured by inclined plane test
Density of hardpan soil	kg/m³	1501	Measurement
Poisson's ratio of hardpan soil	\	0.42	[13]
Bond stiffness of hardpan	N/m³	5×10⁷	[13]
Critical stresses of the bond of hardpan	Pa	4×10⁴	[13]
Shear modulus of hardpan soil	Pa	1×10⁸	[13]
Radius of the bond of hardpan	mm	8.83	[13]
Coefficient of rolling friction in the hardpan soil	\	0.25	Measured by angle of repose test
Coefficient of rolling friction between hardpan soil and 65Mn steel	\	0.14	Measured by inclined plane test
Density of subsoil	kg/m³	1549	Measurement
Bond stiffness of subsoil	N/m³	5×10⁷	[13]
Poisson's ratio of subsoil	\	0.41	[13]
Critical stresses of the bond of subsoil	Pa	3.7×10⁴	[13]
Shear modulus of subsoil	Pa	9×10⁷	[13]
Radius of the bond of subsoil	mm	8.60	[13]
Coefficient of rolling friction in the subsoil	\	0.21	Measured by angle of repose test
Coefficient of rolling friction between subsoil and 65Mn steel	\	0.26	Measured by inclined plane test
Coefficient of restitution between materials	\	0.6	[13]
Coefficient of static friction between soils	\	0.4	[13]
Coefficient of static friction between soil and subsoiler	\	0.5	[4]

3.2 Monitoring soil dynamic behaviors and tillage forces

According to the subsoiler height of 770 mm, the length of cutting share in the vertical direction of 65 mm, working depth of 300 mm and the thickness of hardpan of 130 mm, the length of

ASTL and ASHP in the vertical direction were 170 mm and 65 mm, respectively.   For each section, the effects of wings on disturbance behaviors of soil were monitored using the "Clipping" module in EDEM software.   The tillage forces of different sections of the subsoiler were monitored, respectively, using four 3D measuring boxes in "Selection" module (Figure 6a).   In each measuring box, only the subsoiler was monitored.   The soil disturbance area, i.e., furrow area, in the simulation tests was determined based on the existing method[23,24].   The simulated furrow profile was obtained by connecting the boundary of disturbed soil of different layers (Figure 6b).

To further quantitatively analyze the microscopic disturbance process of soil, representative particles were selected in the transverse center position of the subsoiler L_1, the middle position

of the wing L_2 and the outer edge position of the wing L_3 (Figure 7a).   The depths of particles in every position were 0 mm, 85 mm, 202.5 mm, and 267.5 mm from soil surface; they represented soil surface, middle position of top layer (TL), middle position of hardpan disturbed by arc section (HDAS, 65 mm thick), and middle position of hardpan disturbed by share section (HDSS, 65 mm thick), respectively.   The selected particles were named L_{11}, L_{21}, L_{31}, L_{41}, L_{12}, L_{22}, L_{32}, L_{42}, L_{13}, L_{23}, L_{33} and L_{43} (Figure 7b); and they were used to investigate the displacement variation of soil in L_1, L_2, and L_3 position under the force of winged subsoiler.   By collecting the coordinates of selected particles at different time, the real-time displacements of the selected particles in the x, y, and z directions during subsoiling were determined.
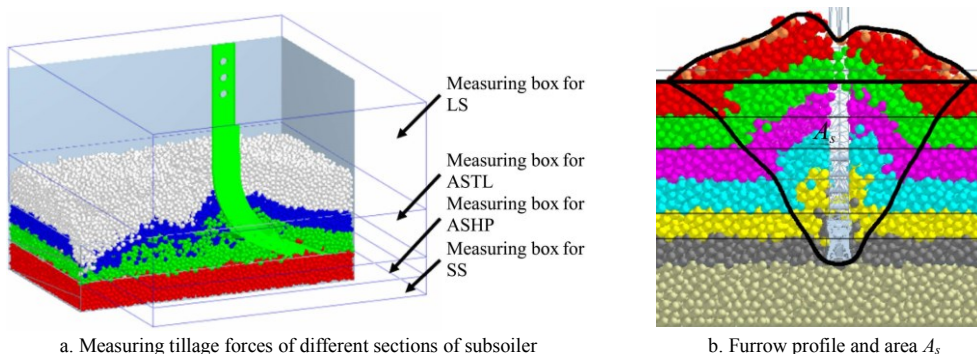
a. Measuring tillage forces of different sections of subsoiler   b. Furrow profile and area A_s

Note: LS, ASTL, ASHP and SS are line section, arc section in the top layer, arc section in the hardpan and share section of the subsoiler, respectively.

Figure 6   Measurement of tillage forces of subsoiler and soil disturbance area
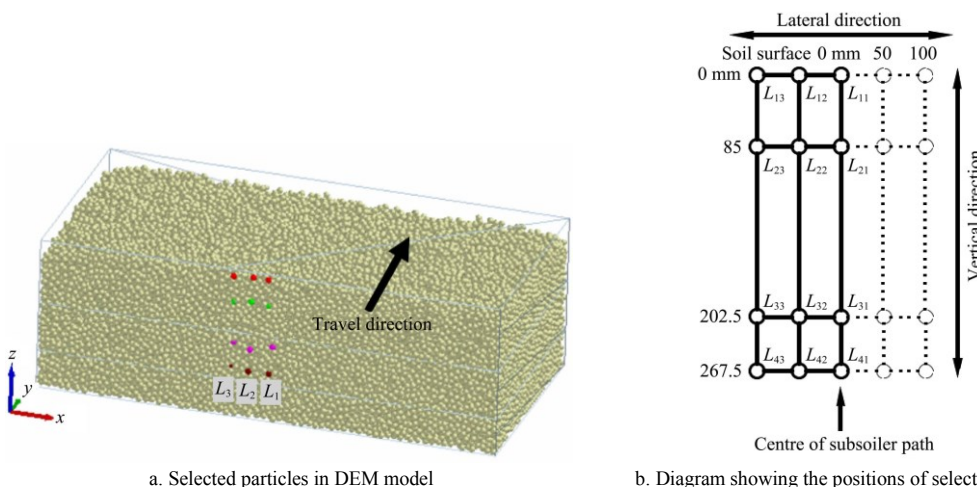
a. Selected particles in DEM model   b. Diagram showing the positions of selected particles

Figure 7   Locations of selected particles

4   Results and discussion

4.1   Soil disturbance characteristics

4.1.1   Microscopic disturbance process of soil

It is difficult to use conventional methods to accurately quantify microscopic soil disturbance below the surface[25].   The number of broken bonds during subsoiling was used to quantitively evaluate the microscopic soil failure (Figure 8).   All bonds in each layer were firstly selected; then the number of broken bonds of every layer in real-time during subsoiling was exported, respectively.   At the same time, longitudinal-sectional views of the soil at four representative moments were obtained using the "Clipping" module in EDEM software (Figure 9).   To quantitatively compare the degree of soil disturbance at different moments, a grid domain was established and soil disturbance area was calculated from the number of grid cells within the disturbed

soil area.
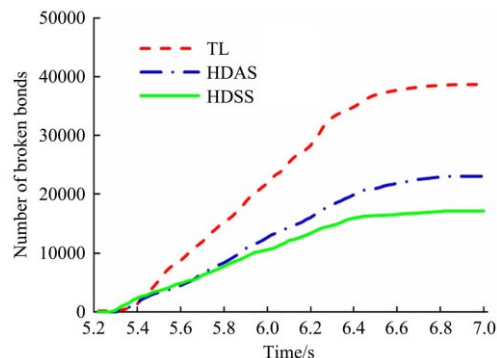
Note: TL is the top layer, HDAS is hardpan disturbed by arc section, and HDSS is hardpan disturbed by share section.

Figure 8   Variation of the number of broken bonds of soil in different positions
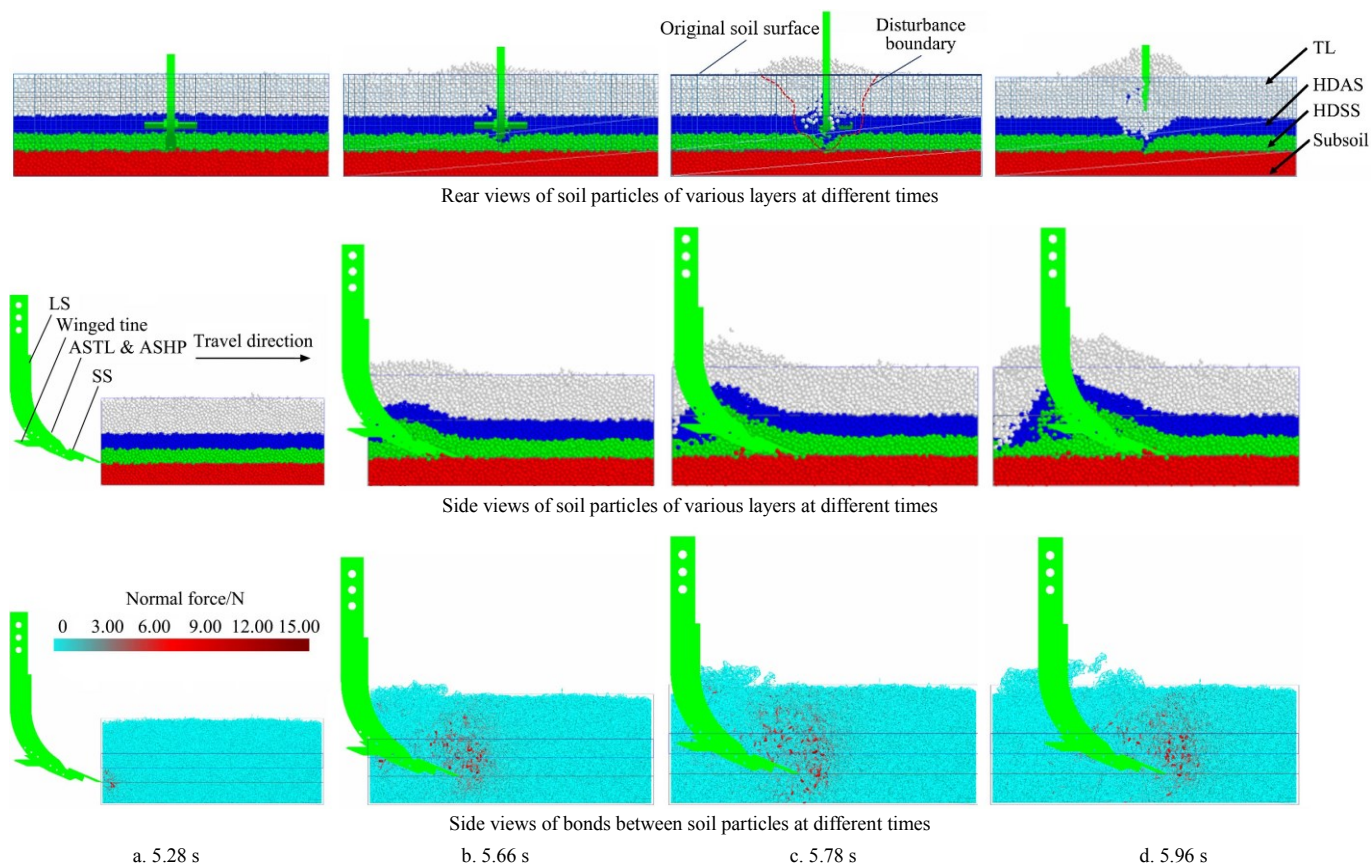
Rear views of soil particles of various layers at different times

Side views of soil particles of various layers at different times

Side views of bonds between soil particles at different times

| a. 5.28 s | b. 5.66 s | c. 5.78 s | d. 5.96 s |

Note: TL is the top layer, HDAS is hardpan disturbed by arc section, and HDSS is hardpan disturbed by share section.   SS represents share section; ASHP represents arc section in the hardpan; ASTL represents arc section in the top layer; LS represents line section.

Figure 9   Soil disturbance behaviors at different times under the action of the winged subsoiler

Bonds breaking of the particles in the model mimicked the soil aggregate breakage resulting from the subsoiler.   The more breakage the soil aggregates, the bigger the number of broken bonds.   As seen from Figures 8 and 9, during the subsoiling process, soil aggregates were broken by the subsoiler continuously and therefore the number of broken bonds increased.   When the subsoiler left the soil bin (>6.80 s), the number of broken bonds became stable.   During the normal subsoiling process of winged subsoiler (>5.78 s), the disturbance range and number of broken bonds of different depths from high to low followed the ranking: TL (white particles), HDAS (blue particles), and HDSS (green particles).   At 5.28 s, with the action of draught force, the cutting share began to shear and compress HDSS soil (Figure 9a).   At this moment, HDSS soil was gradually raised and the number of broken bonds of HDSS started to increase (Figure 8).   At the same time, the TL and HDAS were disturbed by the raised HDSS, which resulted in an increase in the broken bond number of TL and HDAS. Existing studies showed that the area disturbed by the arc-shaped shank and chisel tine usually had a "V" shape[16,17].   Therefore, after 5.28 s, the lateral soil disturbance range of different layers from high to low followed the ranking: TL, HDAS, and HDSS.

With the wings gradually entering soil (Figure 9b), the lateral disturbance range of the HDAS soil was further enlarged since the distance between the two outer edges of the wings (202 mm) was greater than the lateral disturbance width of HDAS soil (160 mm: total width of about 8 grids); additionally, the number of broken bonds in the HDAS soil rapidly increased from 9 to 5515 (Figure 8), indicating that the fragmentation degree of hardpan soil was improved greatly.   Then a soil ridge was gradually formed on the soil surface (Figure 9c).   From 5.66 to 5.78 s, the soil disturbance areas of HDAS and HDSS were increased from 10 600 to

16 800 mm² and from 2600 to 4800 mm², respectively.   This implied that wings were more influential on the disturbance area of HDAS than that of HDSS.   The TL soil started to be broken down under the shearing action of LS; then the disturbed TL soil moved towards the back and bottom of the shank and eventually backfilled the furrow under its own gravity (Figure 9d).   The number of broken bonds of each layer increased until the subsoiling operation finished and then gradually be stable.

Existing studies showed that increasing the disturbance area of deep soil and reducing the disturbance area of top soil helped to improve the soil's water holding capacity[4,5].   It can be seen from the above analysis that wings had a strong influence on the disturbance range and fragmentation degree of the soil above them, but almost no impact on HDSS soil.

4.1.2   Soil disturbance status at different locations

To investigate the effects of winged subsoiler on the disturbance status of soil at different depths and locations, transverse-sectional and longitudinal-sectional views of the soil at 6.24 s (stable working state) were obtained.   The longitudinal and transverse centers of the winged subsoiler shown in Figure 1 were 0 mm location of the transverse-sectional view and longitudinal-sectional view, respectively.   Based on the longitudinal disturbance range and wing length, the distances between longitudinal-sectional views and between transverse-sectional views were set to 40 mm and 50 mm, respectively (Figure 10).

Longitudinal disturbance range and vertical raised height of soil gradually reduced with the increase of the lateral distance between the longitudinal-sectional view and the transverse center of subsoiler (Figure 10a).   This is mainly due to the weaker effect of subsoiler on the farther soil of each layer.   With the shearing and uplifting action of the wings, the HDAS soil at 120 mm and

160 mm was also loosened; however, the HDSS soil at the same distance was almost not affected. This indicated that wings mainly loosened the soil above them, but the soil disturbance degree underneath them was low. As the distance between the transverse-sectional view and longitudinal center of subsoiler increased, the lateral disturbance range and vertical raised height of soil initially increased and then decreased (Figure 10b). At the position of 50 mm, the lateral disturbance range of each layer of soil was the largest. This is mainly due to the fact that the subsoiler width was the largest at this position, and the soil of each layer was affected by the combined action of wings, shank and cutting share.

When comparing Figures 10a and 10b, both longitudinal disturbance range and vertical raised height of soil gradually reduced with the increase of lateral distance between the section view and transverse center of subsoiler. By contrast, lateral disturbance range and vertical raised height of soil firstly increased and then decreased with the increase of longitudinal spacing of the transverse-sectional view and longitudinal center of subsoiler. The lateral disturbance range of soil at different depths within the disturbance range of winged subsoiler followed the ranking: TL, HDAS, and HDSS.

a. Longitudinal-sectional view

0 mm   40 mm   80 mm   120 mm   160 mm

b. Transverse-sectional view

0 mm   50 mm   100 mm   150 mm   200 mm
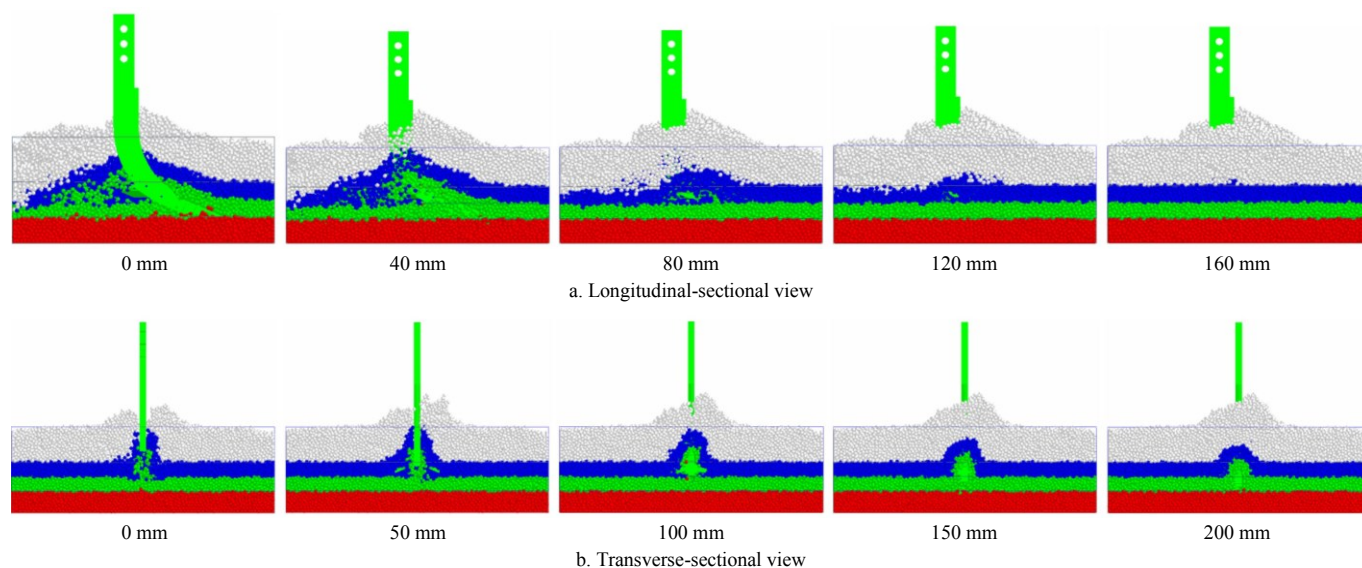
Note: white particles, blue particles, green particles and red particles represent TL, HDAS, HDSS and subsoil, respectively.

Figure 10   Disturbance quality of soil in different layers

4.2   Soil dynamic behaviors

4.2.1   Soil displacement

As shown in Figure 11a, in the lateral direction (x-direction), surface soil particles L_{11}, L_{12}, L_{13}, TL soil particles L_{21}, L_{22}, L_{23}, and HDAS soil particles L_{33} initially moved in the $-x$-direction and then moved in the $+x$-direction. The maximum displacements in the $-x$-direction of surface soils were much larger than that of the soil in other depths. This indicated that the lateral disturbance range of surface soil was relatively large. Moreover, the maximum displacement (-11.08 mm) of L_{23} of TL soil was slightly larger than that (-4.04 mm) of L_{33} of HDAS soil in the $-x$-direction. For HDSS soil, lateral displacements only existed in the positions near the transverse center of winged subsoiler (L_{41} and L_{42}). The above analysis showed that the lateral disturbance range of HDAS soil was significantly enlarged under the action of wings; by contrast, as HDSS soil was only affected by cutting share, its lateral disturbance range was relatively small.

In the travel direction (y-direction), the maximum forward displacements of the soil of L_1 position (L_{11}, L_{21}, L_{31}, L_{41}) and surface soil of L_2 position (L_{12}) were relatively large, followed by TL, HDAS and HDSS soils of L_2 position (L_{22}, L_{32}, L_{42}). By contrast, the forward displacements of surface soil (L_{13}), TL soil (L_{23}), and HDAS soil (L_{33}) of L_3 position were very small; for the HDSS soil of L_3 position (L_{43}), no forward displacement was observed during the entire tillage process. The main reasons were that the soil of L_1 position was directly disturbed by cutting share, shank, and wings, and the shank had the greatest influence on the lateral disturbance range of surface soil[17]. However, surface soil, TL soil, and HDAS soil of L_3 position were only affected by the extruding and cutting action of wings. Neither cutting share nor

wings interfered with the HDSS soil of L_3 position (L_{43}), because of a relatively low position of HDSS soil.

In the vertical direction (z-direction), the vertical displacements of different layers initially increased and then decreased. The maximum vertical displacement of each layer decreased with the increase of lateral distance to the transverse center of the subsoiler. This is due to the fact that during the subsoiling process, the lifted soil that moved towards the back and bottom of the shank and eventually backfilled the furrow; in addition, the extruding, cutting, and uplifting action of winged subsoiler on soil gradually decreased with the increase of lateral distance. Since HDSS soil of L_3 position (L_{43}) was outside the disturbance range of winged subsoiler, there was no vertical displacement for the particle L_{43}.

The lateral disturbance range of soil of different layers followed the ranking: surface soil, TL soil, HDAS soil, and HDSS soil. The winged subsoiler effectively enlarged the lateral disturbance range of the soil near and above the wings. Therefore, optimizing wing installation key parameters, such as proper reduction of the mounting height of wings, could increase the lateral disturbance range of hardpan soil, and then the water-holding capacity of soil can be improved[4,6]. During the subsoiling process, raised soil usually backfilled the furrow under the shearing action of wings and shank. As a result, the forward displacement of each layer initially increased and then decreased in varying degrees with time. Subsoilers resulted in smaller soil forward displacement have many agronomic benefits, such as slighter tillage erosion, less tractor power requirement, and less soil moisture loss[13,26,27]. Therefore, the maximum forward displacement of soil at different locations can be used to evaluate

the performance of subsoilers in terms of agronomic benefits. During subsoiling operation, the arc-shaped shank causes the failure and fragmentation of soil by uplifting and shearing action[5]. However, it is not conducive to reducing the mixing amount of top layer soil and hardpan soil when hardpan soil is uplifted too high, which is considered poor performance for a subsoiler[17]. Thus, by DEM simulation, calculating the maximum vertical displacement of soil at different locations is helpful to study the soil layer mixing for a certain subsoiler.

Existing research focused on optimizing the shape of the shank, e.g., developing a polyline soil-breaking blade subsoiler or bionic subsoiler, to fracture soil effectively and reduce the mixing amount of deep and shallow soil[17,28,29]. However, the impact of wing installation key parameters on the mixing amount of deep and shallow soil was absent in previous DEM studies. Therefore, strengthening the studies on the adaptability of wings will be helpful to the tillage performance improvement of winged subsoiler with an arc-shaped shank.

a. Lateral direction

b. Travel direction

c. Vertical direction
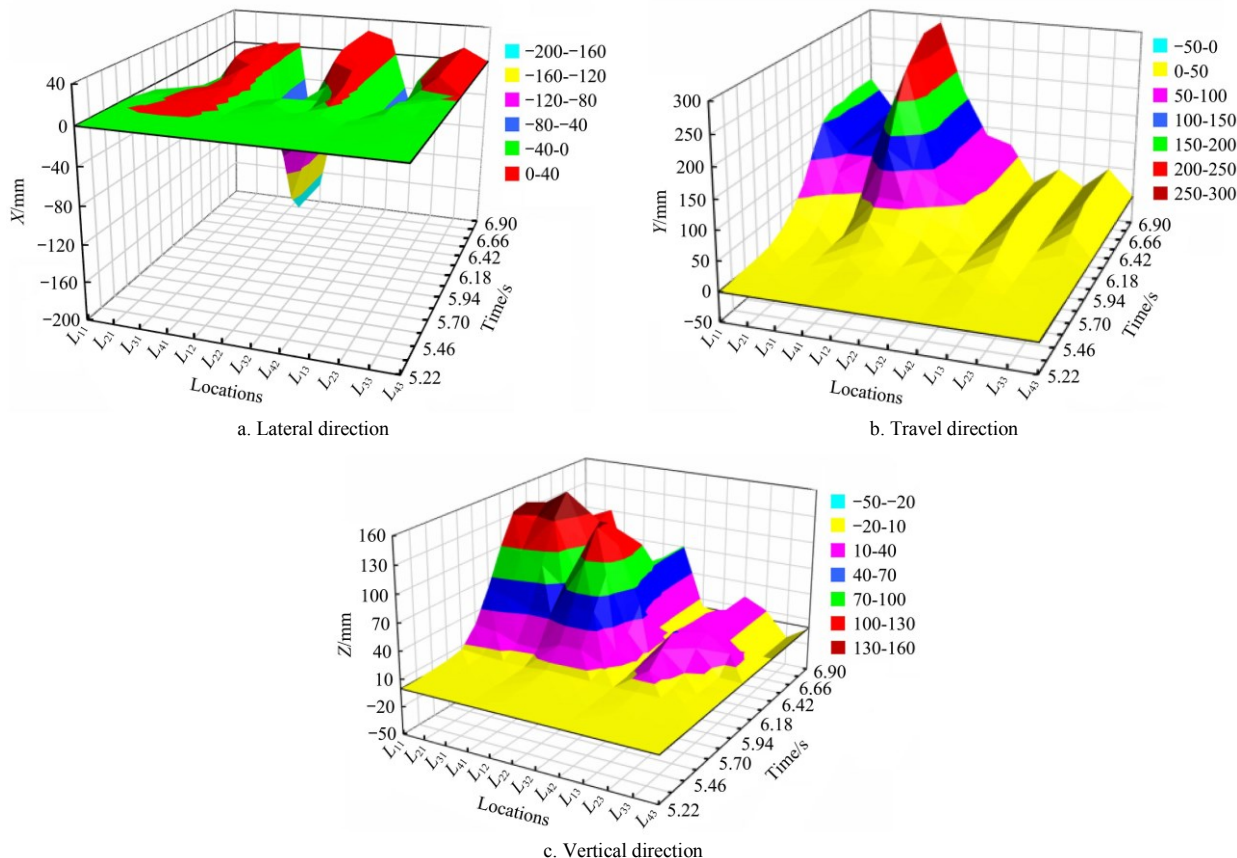
Figure 11   Displacements of representative particles over time

4.2.2   Soil velocity

To investigate the influence of the winged subsoiler on the soil movement of different layers, longitudinal-sectional views of the soil at 5.28 s, 5.66 s, and 5.96 s were selected. The transverse center of the winged subsoiler was 0 mm location of the longitudinal-sectional views and the distance between longitudinal-sectional views was set to 50 mm. The velocity distribution of the soil at different layers and time was compared and analyzed.

When cutting share entered soil (Figure 12a), HDSS soil in the section view of 0 mm moved forward and upward. At the same time, disturbed HDSS soil caused some extrusion on the soil in both sides of the share, increasing the velocity of HDAS soils in both the transverse center of subsoiler (0 mm) and middle position of wings (50 mm). However, the soil at other positions, such as TL, was not disturbed yet due to the limited soil-disturbing capacity of the cutting share. When wings entered soil (Figure 12b), the velocity of the soil near the transverse center of the subsoiler was the highest. At 5.96 s (Figure 12c), the wings were completely buried in soil. For the middle position (50 mm) and the outer edge (100 mm) of wings, the velocity of HDAS soil was relatively high (black particles) because the particles in these two positions were directly affected by wings; by contrast, only a few

particles with fairly low velocities were found in the HDSS at the outer edge of wings.

By comparing the velocity distribution of soil at different layers and time, it could be seen that the winged subsoiler can significantly improve the movement of the soil within the disturbance range of wings. The curve formed by high speed soil particles in the 0 mm section view is similar to the arc curve of the shank.

4.3   Tillage force

Figure 13 shows the simulating curves of tillage force over travel distance. As the winged subsoiler came closer to the soil bin, the draught force of SS was the first one to increase rapidly, followed by ASHP, ASTL, and LS, indicating that different sections of the subsoiler started to disturb soil sequentially (Figure 13). When the winged subsoiler completely entered the soil bin, draught forces of different sections fluctuated around a constant value. On one hand, the fluctuating draught force reflected the breaking of bonds between individual particles as the subsoiler traveled. The bond broke when external normal or tangential stress exceeded the critical stress of a bond[11]. The forces between individual soil particles became zero when the bond was broken[7,11], resulting in fluctuating forces between soil particles, which in turn affected the draught force of the

subsoiler[7].   On the other hand, the soil in front of the winged subsoiler continued to accumulate during the tillage process, which led to the increase of the draught force.   However, when the accumulated soil reached a certain extent, the soil began to fall and then the draught force decreased, resulting in fluctuating of the draught force of the subsoiler[18].   The phenomenon of the

force fluctuation reflected the dynamic nature of soil particles, which was also observed in numerous previous studies[7,18,22,30]. Draught forces of different sections of the subsoiler initially increased rapidly and then decreased rapidly as the subsoiler came out of the soil bin.   The rapidly increased forces are mainly due to the boundary effect[29].
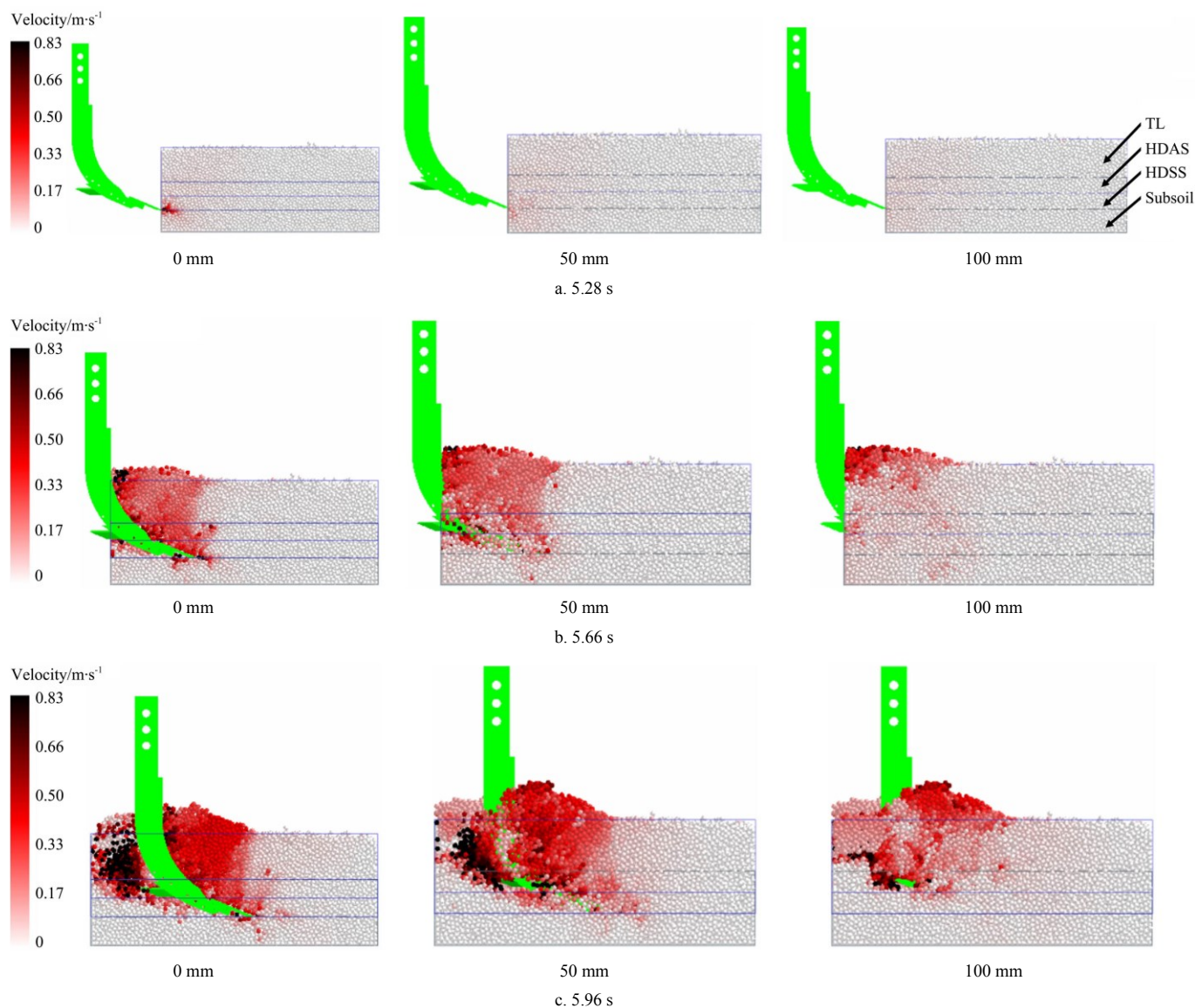
Figure 12   Analysis of soil movement at different positions and time
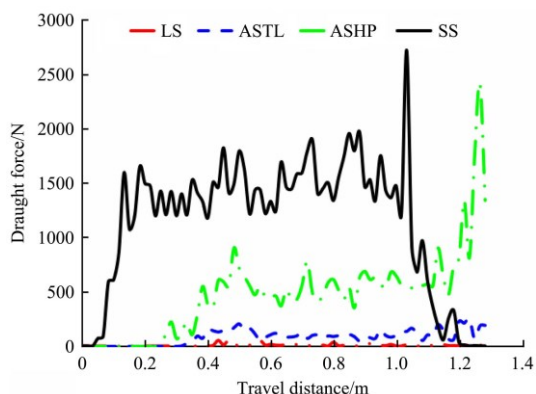
Note: SS represents the share section, ASHP represents the arc section in the hardpan, ASTL represents the arc section in the top layer, and LS represents the line section.

Figure 13   Draught force of different sections of the winged subsoiler during subsoiling

The simulated and experimental draught forces of the non-winged subsoiler over the travel distance are shown in Figure 14.   Both simulated and experimental draught forces initially increased and reached a stable state.   The draught forces from DEM simulation and laboratory test were comparable, which indicated good agreement between the simulation and the experiment.

Force readings were averaged over the stable section of the curves.   The draught forces of SS, ASHP, ASTL and LS were accounted for 69.53%, 25.22%, 4.73% and 0.52% of the total draught force of the winged subsoiler.   Compared to the non-winged subsoiler, the effect of wings on average draught forces of different sections followed the ranking: ASHP, ASTL, SS, and LS (Figure 15a).   The main reasons were that the direct extruding and uplifting action of wings on the HDAS soil intensified the accumulation of the soil in front of the shank.   The wings doubled the vertical force of ASHP.   The vertical force of

ASTL of the winged subsoiler was positive due to the upward movement of soil lifted by the wings (Figure 15b). Both draught and vertical forces of SS were not very sensitive to wings because of the low position of SS. Li[31] found that the draught force of SS of a non-winged subsoiler was more than 80% of the total draught force, which was in line with the results (88.34%) obtained in this study. Both the draught and vertical forces of the LS were low during the entire subsoiling process.

a. DEM simulation
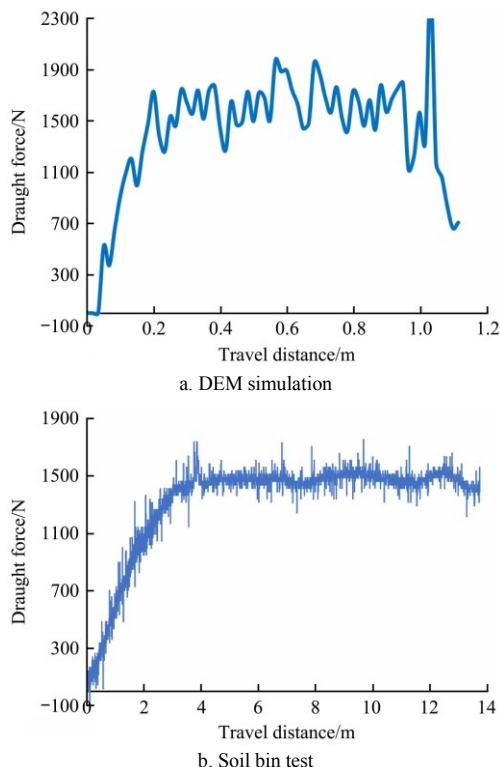
b. Soil bin test

Figure 14   Force-distance curves of the non-winged subsoiler for DEM simulation and soil bin test
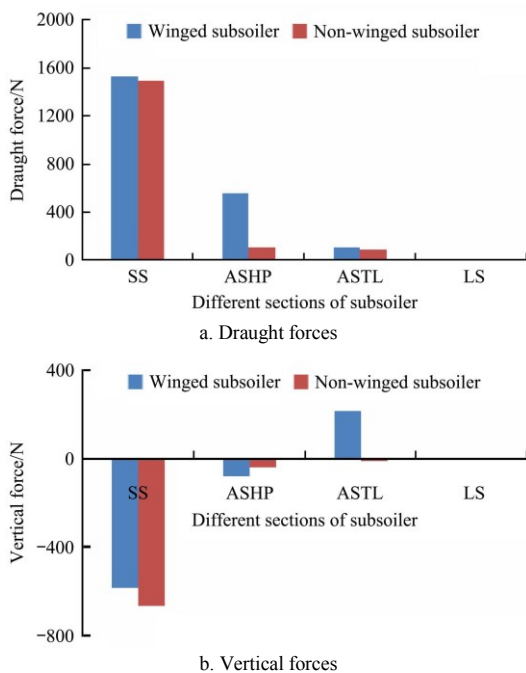
a. Draught forces

b. Vertical forces

Note: SS represents the share section, ASHP represents the arc section in the hardpan, ASTL represents the arc section in the top layer, and LS represents the line section.

Figure 15   Effects of wings on tillage forces of different sections of the subsoiler

4.4   Performance indices analysis

Working depth/tool width ratio is a major variable affecting the type of soil disturbance. According to the study of Godwin[32], tillage tools with a working depth/tool width ratio of less than 5 tend to lose soil in a crescent manner and increasing working depth will change the type of soil disturbance. Working depth (300 mm) in this study is smaller than the critical depth of winged subsoiler, as indicated by a smaller working depth/tool width ratio of 1.49 (<5) and winged subsoiler loosens soil in a crescent manner; in contrast, the working depth is larger than the critical depth of non-winged subsoiler, as indicated by a larger working depth/tool width ratio of 7.5 (>5). To explore the influence of wings on the soil disturbance, the soil cross-section profile of the winged subsoiler and the non-winged subsoiler were compared (Figure 16). An ideal winged subsoiler would expand the disturbance area of the hardpan without significantly increasing the disturbance area of the top layer with the intention of conserving soil and preserving soil moisture[3-6]. Although there was not much difference between winged-subsoiler and non-winded subsoiler in terms of the disturbance area of the top layer, the disturbance area of hardpan by the winged subsoiler was 30% larger than that of non-winged subsoiler. This resulted in a significant increase in soil disturbance area ratio, which was desired.

a. DEM Simulation
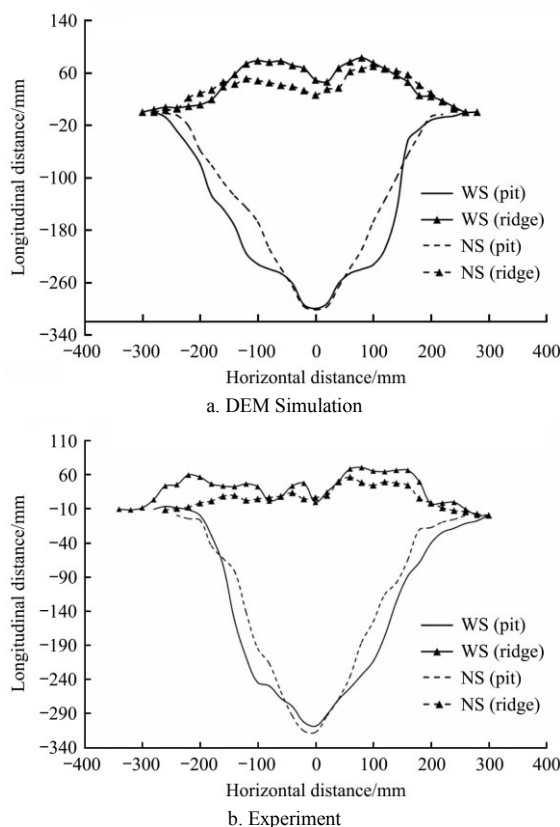
b. Experiment

Figure 16   Comparison of soil disturbance profile curves (WS and NS represent winged and non-winged subsoiler respectively)

According to Equations (1)-(5), simulated and experimental values of five performance indices for the two subsoilers, including soil looseness, soil disturbance coefficient, soil surface flatness, soil disturbance area ratio and soil loosening efficiency, were calculated and compared (Table 2). Relative errors ranging from 3.24% to 41.64% for the winged subsoiler, and a lower range of relative errors (0.24%-28.74%) was found for the non-winged subsoiler. The subsoiler in EDEM software was regarded as a rigid body and therefore the deformation during subsoiling was not considered, which was one of the sources of relative errors between

DEM simulations and experiments. The results between simulations and experiments were basically consistent, which indicated that the DEM models developed in this study had a relatively good accuracy.

Compared with non-winged subsoiler, all performance indices were relatively higher for the winged subsoiler, except for soil loosening efficiency (Table 2). The coefficient of variation of 3 measured soil disturbance areas is 4.74% for winged subsoiler and 3.66% for non-winged subsoiler. Larger soil surface flatness would give rougher soil surface, which is not desirable for the subsequent seeding; however, the rough soil surface is effective to reduce soil erosion[15]. The wings were able to directly break the hardpan soil and increase its disturbance area, which led to the increase of soil disturbance area ratio. A larger soil disturbance area ratio is considered better performance for a subsoiler which

tends to improve the water-holding capacity of the soil[6]. Adding wings to the subsoiler gave a 36% increase in draught force which was supported by the study of Spoor and Godwin[33] who reported that the addition of wings increased the draught force by approximately 30%; however, Li et al.[34] found that adding wings to a subsoiling tool doubled the draught force. The phenomenon is possibly due to the differences in the tool geometry which greatly affect the tool performance. For example, the winged subsoiler has higher soil loosening efficiency only at smaller rake angles for a given tool geometry[34]. Additionally, the variation of the installation parameters (e.g. mounting height of subsoiler's wing) would make a significant difference to the performance of the winged subsoiler[6,24,33]. A comprehensive consideration of key installation parameters of wings is therefore essential to improve the overall performance of the winged subsoiler.

Table 2   Performance indices

Parameter	Winged subsoiler			Non-winged subsoiler		
	Simulation	Experiment	Error/%	Simulation	Experiment	Error/%
Soil looseness/%	17.05	15.83	7.71	14.67	11.57	26.79
Soil disturbance coefficient/%	56.69	58.59	3.24	54.39	54.26	0.24
Soil surface flatness/mm	28.03	19.79	41.64	19.44	15.10	28.74
Furrow width/mm	480.20	448.65	7.03	441.32	418.13	5.55
Soil loosening efficiency/mm^2·N	37.15	39.35	5.59	42.44	46.27	8.28
Soil disturbance area ratio	0.3613	0.3835	5.79	0.2898	0.3443	15.83
Draught force/N	2198.63	2003.98	9.71	1692.75	1470.97	15.08

Existing research has demonstrated that a small disturbed area of top layer soil and increasing the disturbed area of the hardpan soil is favorable for improving water-holding capacity of soil[4,6]. Based on the soil disturbance profile curves (Figure 16), the simulated and experimental disturbed area of the TL soil, HDAS soil and HDSS soil were determined (Figure 17). A larger soil disturbed area was found for the winged subsoiler than that for the non-winged subsoiler; adding wings to an arc-shaped subsoiler increased the disturbance area of HDAS, TL and HDSS by 47.52%, 7.74% and 4.59%, respectively, indicating that the disturbance of the HDAS soil was improved effectively by wings. The average errors between the simulated and experimental disturbed area of different layers for the winged and non-winged subsoiler were 10.63% and 9.62%, respectively, which again validated the DEM simulations.
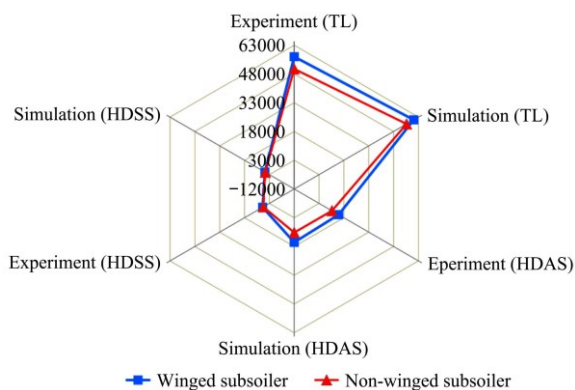
Note: TL represents top layer, HDAS represents hardpan disturbed by arc section, and HDSS represents hardpan disturbed by share section.

Figure 17   Radar map of the simulated and measured soil disturbance area of different layers (mm^2)

5   Conclusions

A DEM model was developed to simulate soil-subsoiler

interactions. The model was validated by the experimental data of soil disturbance. Through simulations, the impact of winged and non-winged subsoilers on soil dynamic characteristics was investigated. The following conclusions were drawn:

1) The wings mainly affected the disturbance range and fragmentation degree of the soil above them. For the winged subsoiler, the lateral disturbance range of the soil at different depths followed the ranking: top layer (TL), hardpan disturbed by arc section (HDAS), and hardpan disturbed by share section (HDSS). Adding wings to an arc-shaped subsoiler increased the disturbance area of HDAS, TL and HDSS by 47.52%, 7.74% and 4.59%, respectively.

2) The winged subsoiler can significantly improve the movement of the soil within the disturbance range of the wings. The curve formed by soil particles with higher speed at the section view of the subsoiler's transverse center was similar to the arc curve of the shank.

3) The draught forces of share section (SS), arc section in the hardpan (ASHP), arc section in the top layer (ASTL) and line section (LS) accounted for 69.53%, 25.22%, 4.73% and 0.52% of the total draught force of the winged subsoiler. The wings had the greatest influence on the draught force of ASHP (a 430.34% increase), followed by the draught force of ASTL (a 13.74% increase). Adding wings to an arc-shaped subsoiler gave a 36% increase in total draught force.

4) Compared with non-winged subsoiler, winged subsoiler had higher soil looseness (15.83%), soil disturbance coefficient (58.59%), furrow width (448.65 mm) and soil disturbance area ratio (0.3835), but poorer soil surface flatness (19.79 mm) and lower soil loosening efficiency (39.35 mm²/N).

5) The simulated and experimental results were basically consistent, indicating that the DEM was able to simulate the subsoiling process of the subsoilers with a reasonably good accuracy.

The results provided critical information in designing and optimizing winged subsoilers on aspects of improving soil loosening effectiveness and reducing draught force of the winged subsoiler. To improve the research, future studies need to consider addressing the technical problems of continuous time-dependent measurements of particle positions during the experiments.

Acknowledgements

Nomenclature

a_{kj}	vertical distance from the j-th measured point on the soil surface after tillage to horizontal reference line in the k-th measurement, mm
A_f	area between soil surface after tillage and theoretical subsoiling bottom before subsoiling, mm²
A_h	soil disturbance area of the hardpan, mm²
A_o	area between original soil surface and theoretical subsoiling bottom before subsoiling, mm²
A_s	soil disturbance area between original soil surface and internal soil disturbance profile, mm²
A_t	soil disturbance area of the top layer, mm²
b	wing width, mm
d_0	spacing between two adjacent points, mm
F_d	draught force of the subsoiler, N
h	mounting height of wings, mm
H	subsoiler height, mm
l_0	furrow width, mm
l_1	share length, mm
l_2	subsoiler width, mm
l_3	wing length, mm
L_1	transverse center position
L_2	middle position of the wings
L_3	outer edge position of the wings
n_k	number of test points in the k-th measurement
P	the soil looseness, %
R	radius of curvature of the shank, mm
S_k	soil surface flatness in the k-th measurement, mm
t	wing thickness, mm
κ	soil disturbance area ratio

Greek letters

α	rake angle, (°)
β	mounting angle of wings, (°)
λ	soil disturbance coefficient, %
θ	backward angle of wings, (°)
η	soil loosening efficiency, mm²/N

[References]

[1] Khalilian A, Han Y J, Marshall M W, Gorucu S. Abbaspour-Gilandeh Y, Kirk K R. Evaluation of the Clemson instrumented subsoiler shank in coastal plain soils. Computers and Electronics in Agriculture, 2014; 109: 46–51.

[2] Shahgoli G, Saunders C, Desbiolles J M A, Fielke J. The effect of oscillation angle on the performance of oscillatory tillage. Soil and Tillage Research, 2009; 104(1): 97–105.

[3] Zeng Z, Chen Y, Zhang X. Modelling the interaction of a deep tillage tool with heterogeneous soil. Computers and Electronics in Agriculture, 2017; 143: 130–138.

[4] Hang C, Gao X, Yuan M, Huang Y, Zhu R. Discrete element simulations and experiments of soil disturbance as affected by the tine spacing of subsoiler. Biosystems Engineering, 2018; 168(S1): 73–82.

[5] Huang Y, Hang C, Yuan M, Wang B, Zhu R. Discrete element simulation and experiment on disturbance behavior of subsoiling. Transactions of the CSAM, 2016; 47(7): 80–88. (in Chinese)

[6] Xia L. Optimum design and experimental study shovel wing based on discrete element method. Master dissertation. Yangling: Northwest A&F University, 2018; 80p. (in Chinese)

[7] Chen Y, Munkholm L, Nyord T. A discrete element model for soil-sweep interaction in three different soils. Soil and Tillage Research, 2013; 126: 34–41.

[8] Ucgul M, Fielke J, Saunders C. 3D DEM tillage simulation: validation of a hysteretic spring (plastic) contact model for a sweep tool operating in a cohesionless soil. Soil and Tillage Research, 2014; 144: 220–227.

[9] Wang X, Zhang S, Pan H, Zheng Z, Huang Y, Zhu R. Effect of soil particle size on soil-subsoiler interactions using the discrete element method simulations. Biosystems Engineering, 2019; 182: 138–150.

[10] Ucgul M, Saunders C, Fielke J. Comparison of the discrete element and finite element methods to model the interaction of soil and tool cutting edge. Biosystems Engineering, 2018; 169: 199–208.

[11] Ding Q, Ren J, Adam B, Zhao J, Ge S, Li Y. DEM analysis of subsoiling process in wet clayey paddy soil. Transactions of the CSAM, 2017; 48(3): 38–48. (in Chinese)

[12] Tanaka H, Oida A, Daikoku M, Lnooku K, Sumikawa O, Nagasaki Y, et al. DEM simulation of soil loosening process caused by a vibrating subsoiler. Agricultural Engineering International: the CIGR Ejournal, 2007; 9: 1–18.

[13] Wang X, Yue B, Gao X, Zheng Z, Zhu R, Huang Y. Discrete element simulations and experiments of disturbance behavior as affected by mounting height of subsoiler's wing. Transactions of the CSAM, 2018; 49(10): 124–136. (in Chinese)

[14] Zhang J, Yan X, Lin Z, Zhu R. Design and experiment of self-exciting vibration deep-loosening and sub-soiling machine. Transactions of the CSAM, 2016; 47(9): 44–49. (in Chinese)

[15] Li B, Chen Y, Chen J. Modeling of soil-claw interaction using the discrete element method (DEM). Soil Tillage Research, 2016; 158: 177–185.

[16] Li X, Fu J, Zhang D, Cui T, Zhang R. Experiment analysis on traction resistance of vibration subsoiler. Transactions of the CSAE, 2012; 28(1): 32–36. (in Chinese)

[17] Zheng K, He J, Li H, Dao P, Wang Q, Zhao H. Research on polyline soil-breaking blade subsoiler based on subsoiling soil model using discrete element method. Transactions of the CSAM, 2016; 47(9): 62–72. (in Chinese)

[18] Li B, Liu F, Mu J, Chen J, Han W. Distinct element method analysis and field experiment of soil resistance applied on the subsoiler. Int J Agric & Biol Eng, 2014; 7(1): 54–59.

[19] Beakawi Al-Hashemi H, Baghabra Al-Amoudi O. A review on the angle of repose of granular materials. Powder Technology, 2018; 330: 397–417.

[20] Wei D, Wang J, Zhao B. A simple method for particle shape generation with spherical harmonics. Powder Technology, 2018; 330: 284–291.

[21] Mak J, Chen Y, Sadek M. Determining parameters of a discrete element model for soil–tool interaction. Soil and Tillage Research, 2012; 118: 117–122.

[22] Ucgul M, Saunders C, Fielke J. Discrete element modelling of top soil burial using a full scale mouldboard plough under field conditions. Biosystems Engineering, 2017; 160: 140–153.

[23] Barr J B, Ucgul M, Desbiolles J M A, Fielke J. Simulating the effect of rake angle on narrow opener performance with the discrete element method. Biosystems Engineering, 2018; 171: 1–15.

[24] Wang X, Gao P, Yue B, Shen H, Fu Z, Zheng Z, et al. Optimisation of installation parameters of subsoiler' wing using the discrete element method. Computers and Electronics in Agriculture, 2019; 162: 523–530.

[25] Hang C, Huang Y, Zhu R. Analysis of the movement behavior of soil between subsoilers based on the discrete element method. Journal of Terramechanics, 2017; 74: 35–43.

[26] Gursoy S, Chen Y, Li B. Measurement and modelling of soil displacement from sweeps with different cutting widths. Biosystems Engineering, 2017; 161: 1–13.

[27] Solhjou A, Fielke J, Desbiolles JMA. Soil translocation by narrow openers with various rake angles. Biosystems Engineering, 2012; 112(1): 65–73.

[28] Guo Z, Zhou D, Zhou Z. Simulation research on mechanical

performances of several kinds of cultivating components with different soil-engaging surfaces. Journal of Mechanical Engineering, 2010; 46: 71–75. (in Chinese)

[29] Sun J, Wang Y, Ma Y, Tong J, Zhang Z.   DEM simulation of bionic subsoilers (tillage depth>40 cm) with drag reduction and lower soil disturbance characteristics.   Advances in Engineering Software, 2018; 119: 30–37.

[30] Shmulevich I.   State of the art modeling of soil-tillage interaction using discrete element method.   Soil and Tillage Research, 2010; 111(1): 41–53.

[31] Li B.   Reducing force and tillage performance of a subsoiler based on the discrete element method (DEM).   Doctoral dissertation.   Yangling: Northwest A&F University, 2016; 126p. (in Chinese)

[32] Godwin R J.   A review of the effect of implement geometry on soil failure and implement forces.   Soil and Tillage Research, 2007; 97(2): 331–340.

[33] Spoor G, Godwin R J.   An experimental investigation into the deep loosening of soil by rigid tines.   Journal of Agricultural Engineering Research, 1978; 23: 243–258.

[34] Li B, Chen Y, Chen J.   Comparison of two subsoiler designs using the discrete element method (DEM).   Transactions of the ASABE, 2018; 61(5): 1529–1537.